Supporting Information

Fabrication of ZnMn$_2$O$_4$@ZnIn$_2$S$_4$ Ball-in-Ball Hollow Microspheres

as an Efficient Photocatalyst for Hydrogen Evolution

Lijun Liu, Wenya Tang, Luyang Zuo, Huitao Fan*, Bo Li, Liya Wang*

College of Chemistry and Pharmaceutical Engineering, Nanyang Normal University, Nanyang, 473601, PR China

E-mail addresses: fanhuitao818@nynu.edu.cn (H. Fan), wly@nynu.edu.cn (L. Wang).

Characterizations

Samples morphology and structure were examined using field emission scanning electron microscopy (FESEM, Zeiss Sigma–500) and transmission electron microscopy (TEM, JEOL JEM-2100F) equipped with an energy-dispersive X-ray (EDX) elemental mapping. Powder X-ray diffraction (PXRD, Bruker D8 Advance X-ray diffractometer with Cu-Kα radiation) data of the samples were collected. N_2 sorption analysis were carried out on an ASAP 2020 instrument (Micromeritics, USA). The specific surface areas were determined by the Brunaner Emmett Teller (BET) technology through 3Flex (Micromeritics, USA) software, and the pore size distributions were identified by the adsorption branch of the isotherm. Utilizing 284.6 eV (C 1s peak) as a reference, surface chemical states were examined using XPS (Thermo Scientific K-Alpha, USA). With the use of an inductively coupled plasma-optical emission spectrometer (ICP-OES, ICPE 9820, Japan), the actual Mn ratios in the ZMOZ composites were determined, and concentrated hydrochloric acid and concentrated nitric acid were used to create the digesting solution. The UV–vis diffuse reflectance spectra (UV-vis DRS, Hitachi UH4150 UV–visible spectrophotometer) of the samples were also detected. PL spectra and the TRPL spectrum were obtained using the Edinburgh Analytical Instruments FLS980 spectrometer. The surface potential of the sample was tested using Atomic Force Microscope-Kelvin Probe Force Microscope (AFM-KPFM) method with potential model (Bruker Dimension Icon). Surface photovoltage spectra (SPV) were recorded on an CEL-SPS 1000 system (Beijing China Education Au-light Co., Ltd.).

Photocatalytic hydrogen evolution test

In the photocatalytic hydrogen evolution study, from Beijing Perfect Light Co., Ltd. purchased the Labsolar-6AG online photocatalytic system was used for hydrogen production tests and cycle tests, and a 300 W xenon lamp equipped with a 400 nm cutoff filter (PLS-SXE300) as the light source. Before the experiment, the reactor was thoroughly degassed for 30 min to eliminate any air. Then, using gas chromatography (Shanghai Kechuang, GC910), the resultant H_2 was observed. 3 mL of TEOA was used as a sacrificial reagent in a typical technique to add a solution including 27 mL

of deionized water was mixed with the photocatalyst (5 mg).

The Apparent quantum efficiencies (AQE) for photocatalytic hydrogen evolution were measured using different monochromatic light filters (380, 400, 420, 450 nm), and the power meter (Thorlabs PM100D) was used to measure the number of incident photons. The following equation was utilized to calculate the AQE:

$$AQE = \frac{number\ of\ evolved\ hydrogen\ molecules \times 2}{number\ of\ incident\ photons} \times 100\%$$

Photoelectrochemical measurements

The standard three-electrode cell on a CHI660E electrochemical workstation was utilized to investigate the photoelectrochemical performance. A photocatalyst electrode coated on a glassy carbon electrode served as the working electrode, a Pt plate served as the counter electrode, an Ag/AgCl electrode in saturated KCl served as the reference electrode, and the Na_2SO_4 (0.5 mol L^{-1}) solution was the electrolyte. A mixed solution containing 950 μL mixture of photocatalyst and alcohol, and 50 μL Nafion solution was used to prepare the working electrodes. Following a one-hour ultrasonic, the mixed solution was placed onto the glassy carbon electrode and allowed to dry at room temperature. At the open circuit potential circumstances, the frequency range of 10^5 to 0.1 Hz has been constructed for the electrochemical impedance spectroscopy (EIS) and the transient photocurrent corresponding test was conducted using a 300 W xenon lamp with a UV-CUT filter ($\lambda \geq 400$ nm). To assess the flat-band potential of prepared ZMO and ZIS, Mott-Schottky (M–S) curves have been performed at frequencies of 1.5, 1.0, and 0.5 kHz.

Method and computational details

All DFT calculations were performed using the Vienna Ab initio Simulation Package (VASP). Where we compute the projected affixed plus plane wave (PAW) and generalized gradient approximation (GGA) exchange correlation generalizations using the PBE formulation. In the structure optimization calculations ionic nuclei and valence electrons are operated on the basis of the projected augmented plane wave potential and the plane wave with a cutoff energy of 400 eV, respectively. The Monkhorst-Pack method was used for sampling in the Brillouin zone. The

convergence criteria used for the energy and force calculations were set to 10^{-5} eV and 0.02 eV/Å, respectively. When the energy change is less than 10^{-5} eV, the electrons are considered to be self-consistent. The geometric optimization is considered to be converged when the energy change is less than 0.02 eV/Å. In this work, the ZIS (102) surface and the ZMO (200) surface are modeled, respectively. Based on the two models, a vacuum layer with Z-direction of > 20 Å is established and the work function is calculated, which is given by $E_w = E_{Vac} - E_f$. The vacuum layer serves to avoid interactions between neighboring configurations. The size of the ZIS (102) surface model is $2 \times 2 \times 1$ in the X, Y, Z direction and is set to 3 atomic layers. The same size of ZMO (200) is $2 \times 2 \times 1$, and the number of atomic layers is set to 3. In the structural optimization and static self-consistent calculation of the material model, the ZIS (102) and ZMO (200) surface Brillouin zone integration and electronic properties are used in the $1 \times 5 \times 1$ and $4 \times 3 \times 1$ gamma point center k–point   grids,   respectively.
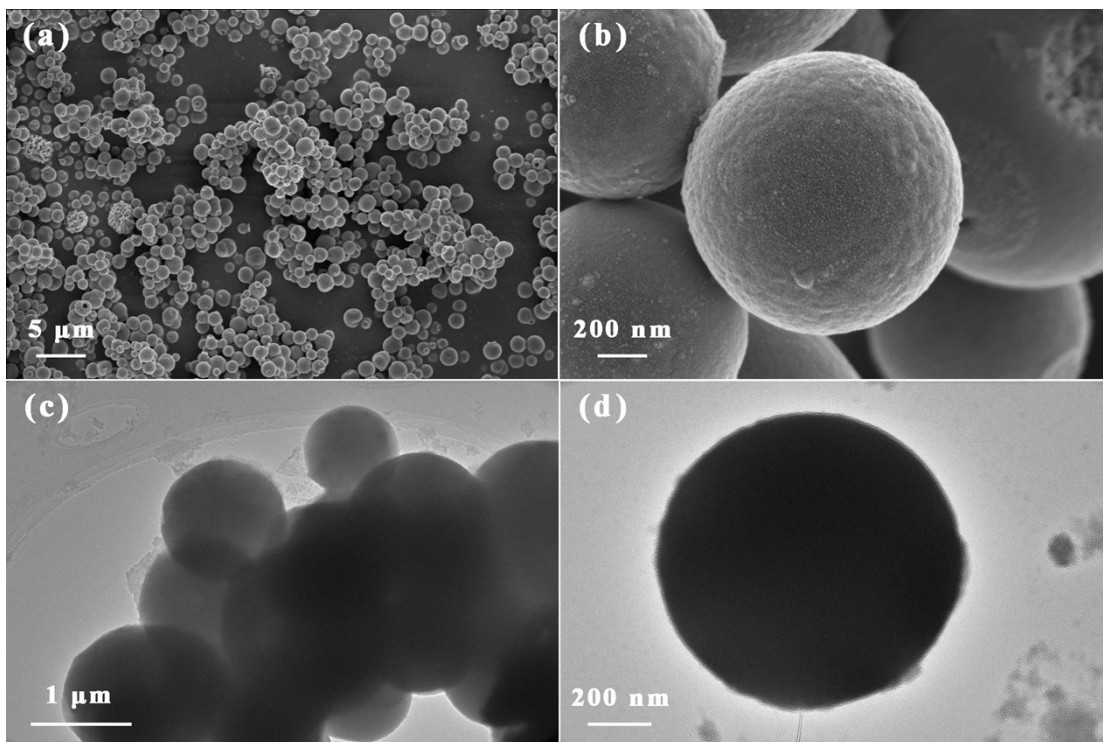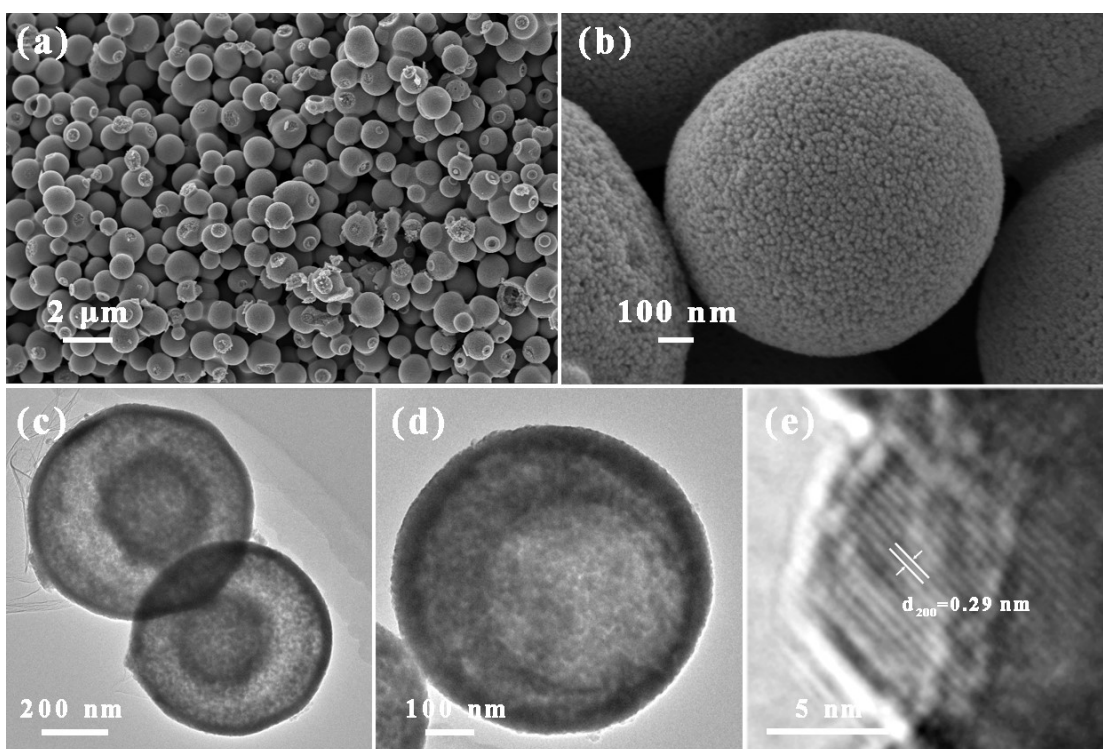
Figure S1. (a, b) FESEM and (c, d) TEM images of ZnMn-glycolate.

Figure S2. (a, b) FESEM, (c, d) TEM, (e) HRTEM of ZMO ball-in-ball hollow microspheres.
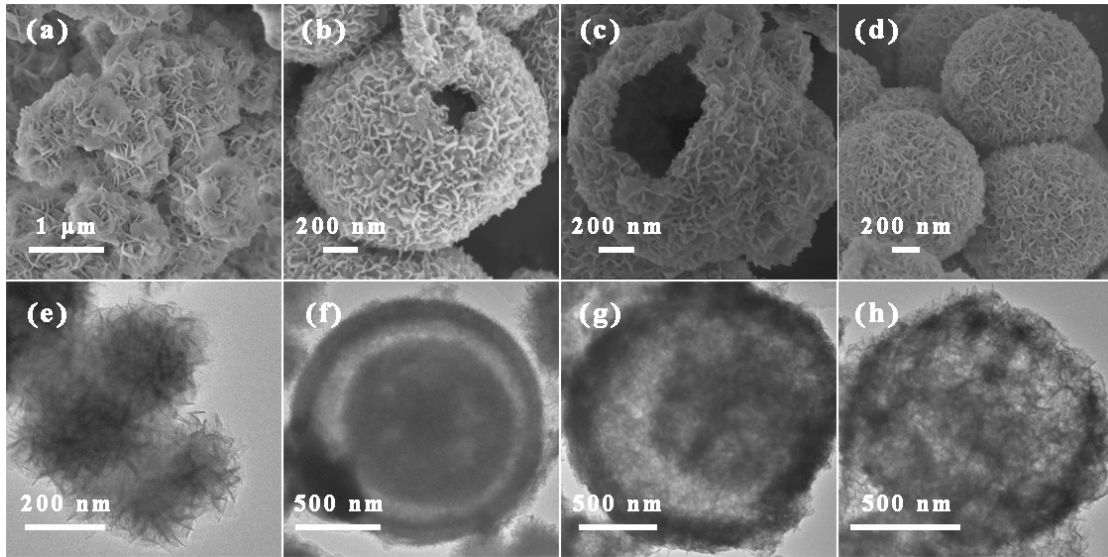
Figure S3. FESEM and TEM images of ZIS and ZMOZ obtained with different amounts of ZMO: (a, e) ZIS, (b, f) 5% ZMOZ, (c, g) 15% ZMOZ, (d, h) 20% ZMOZ.
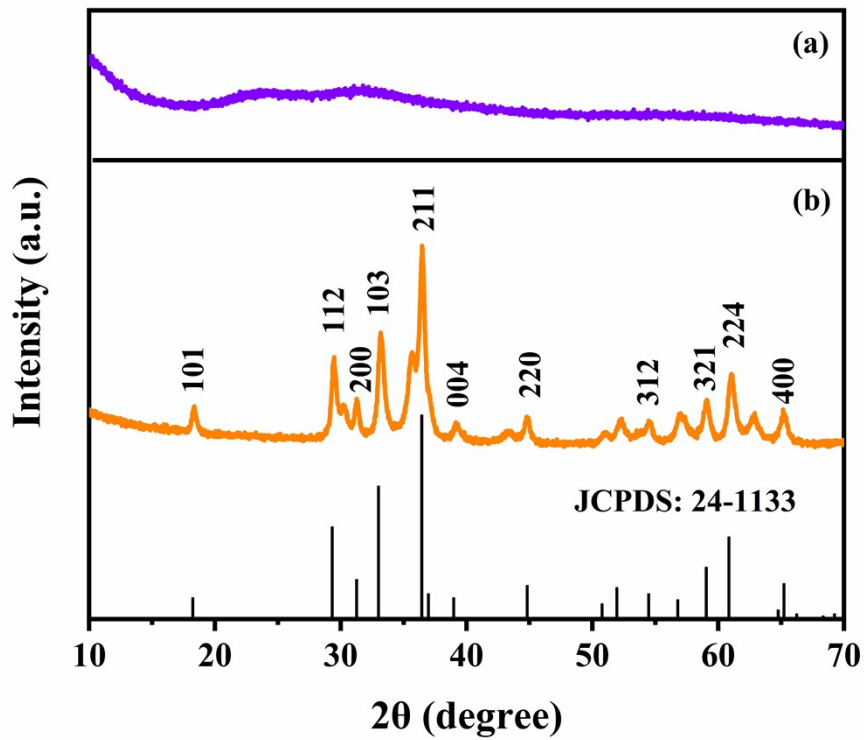

Figure S4. PXRD patterns of the as-synthesized (a) ZnMn-glycolate precursor and (b) ZMO product annealed at 500 °C in air for 4 h with a heating rate of 1 °C min^{-1}.
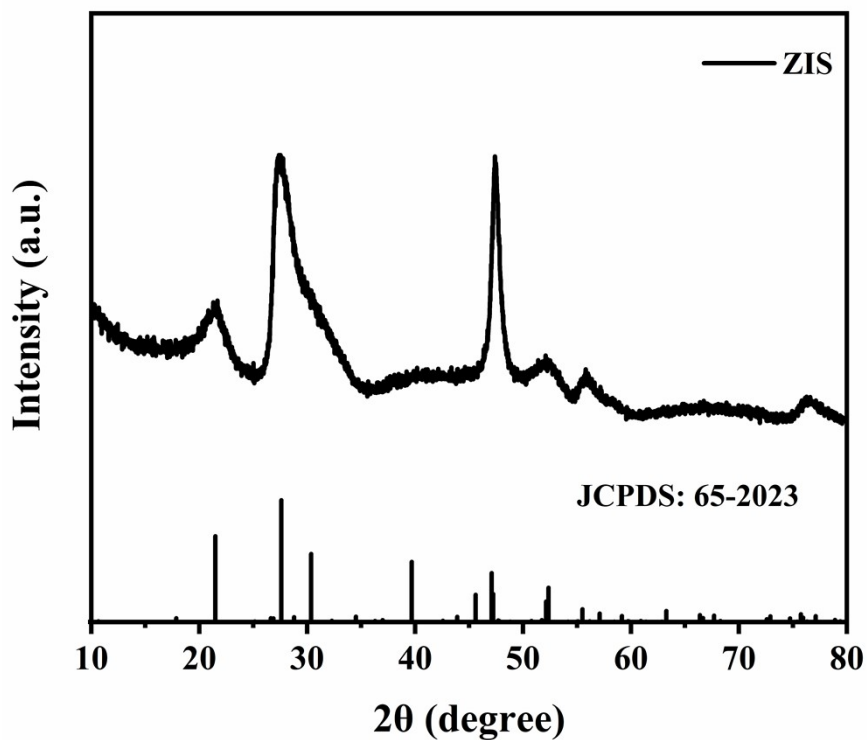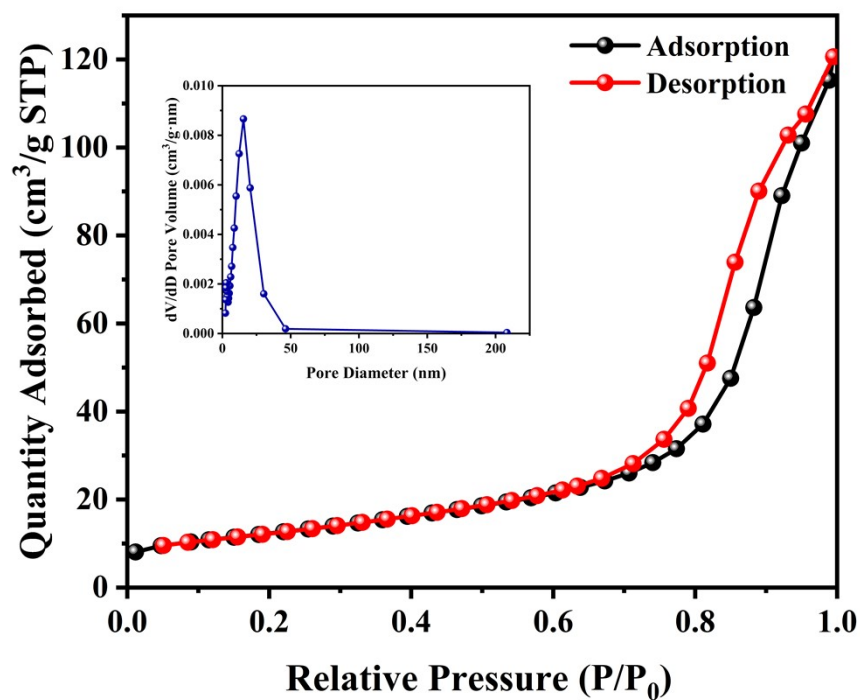
Figure S5. PXRD pattern of pure ZIS.

Figure S6. N_2 sorption isotherms and the corresponding pore size distribution of ZMO.
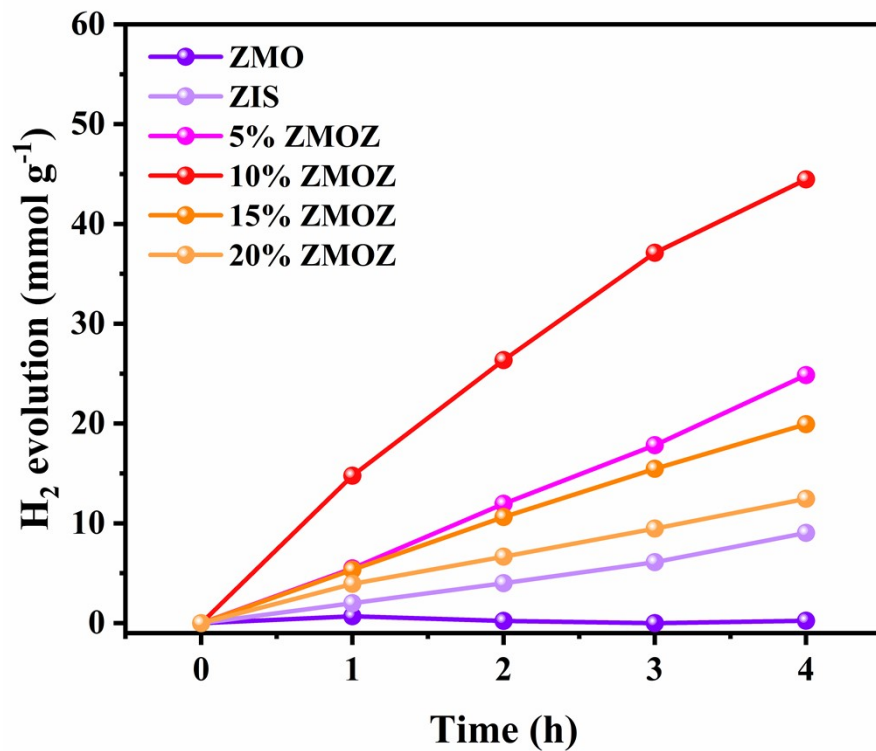
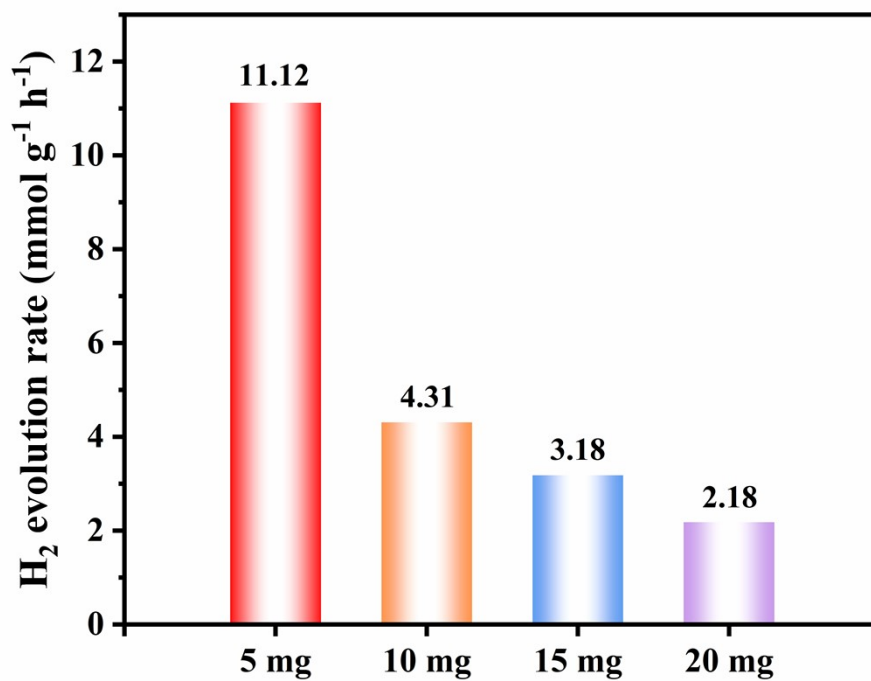**Figure S7.** PHE performances with increasing time.

Figure S8. PHE rates of 10% ZMOZ with different amounts as photocatalysts.

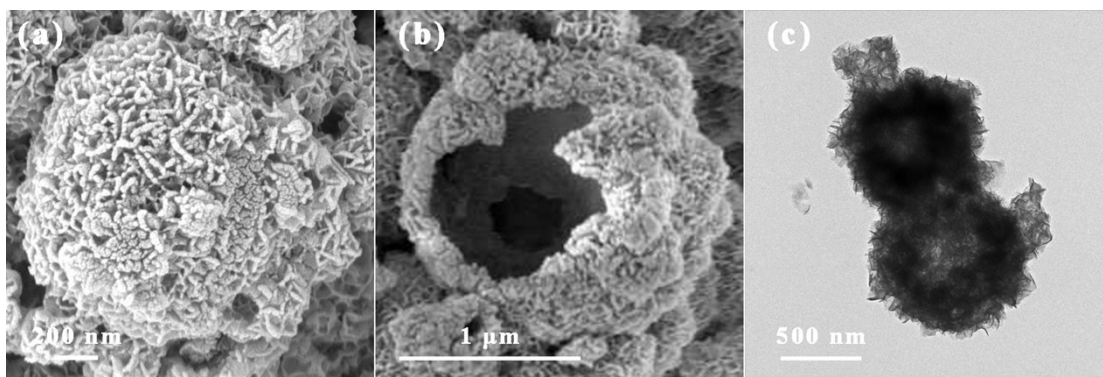**Figure S9.** (a, b) FESEM images, and (c) TEM images of 10% ZMOZ after 4 h photocatalytic reactions.
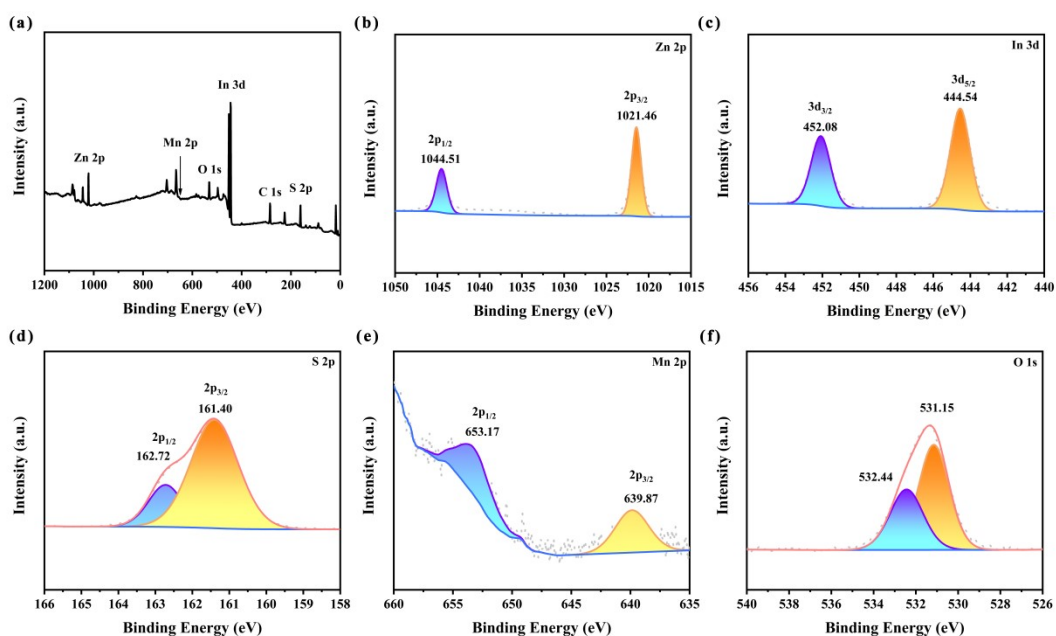
Figure S10. (a) XPS survey spectra and XPS high-resolution spectra of (b) Zn 2p, (c) In 3d, (d) S 2p, (e) Mn 2p, and (f) O 1s of 10% ZMOZ after 4 h photocatalytic reactions.
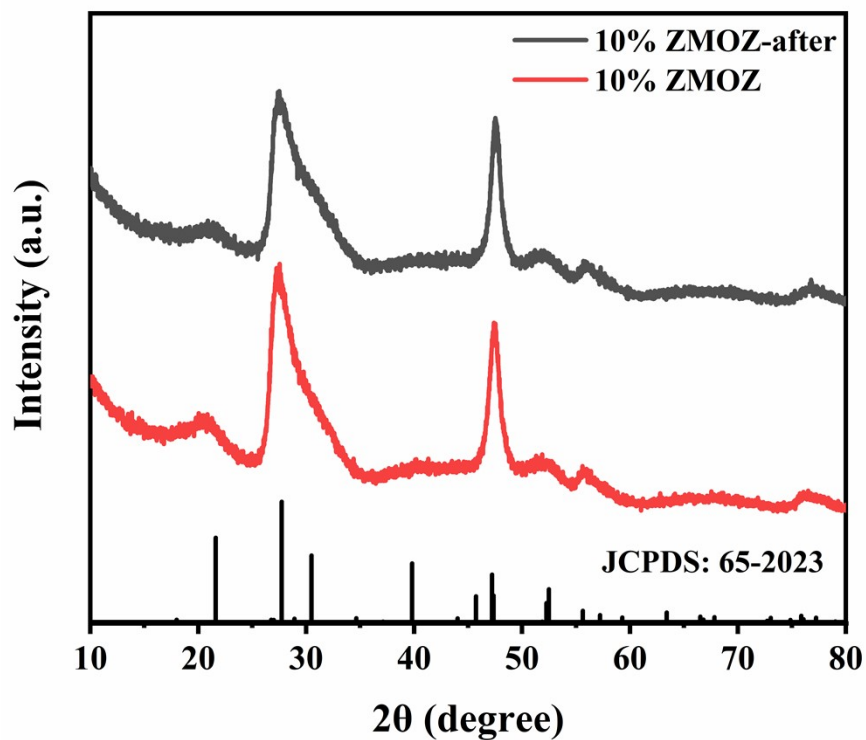
Figure S11. 10% ZMOZ before and after photocatalytic H$_2$ evolution reactions.

Figure S12. M-S plot of 10% ZMOZ composite photocatalysts.

Figure S13. Photocatalytic H_2 evolution performance of 10% ZMOZ for different sacrificial agents.

Figure S14. Photocatalytic H_2 evolution performance of 10% ZMOZ for different preparation methods.

Table S1. Comparison of representative $ZnIn_2S_4$-based photocatalysts for H_2 evolution efficiency.

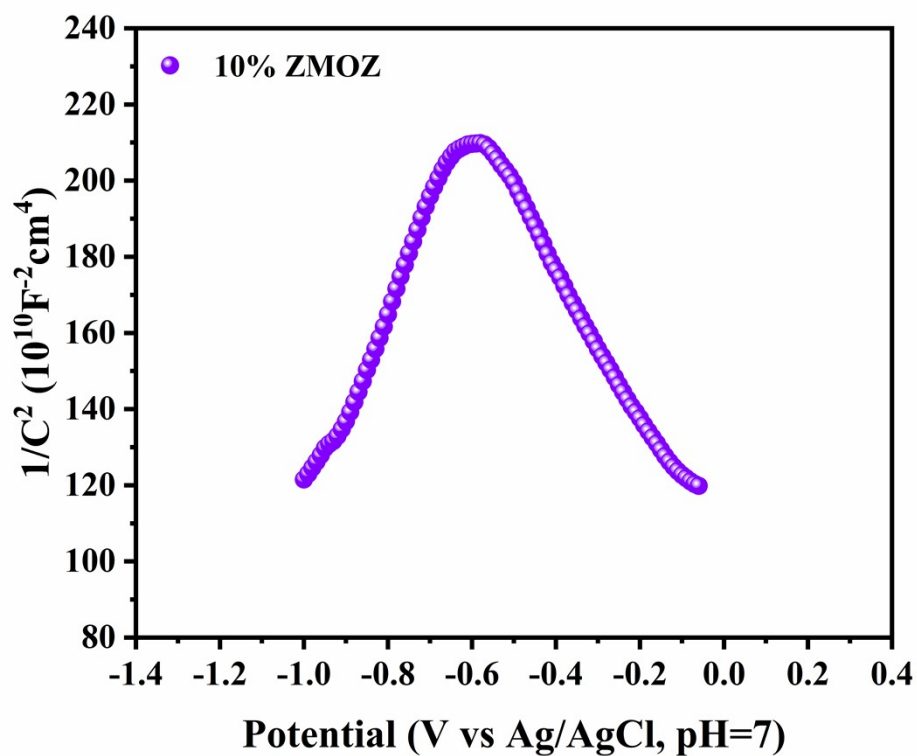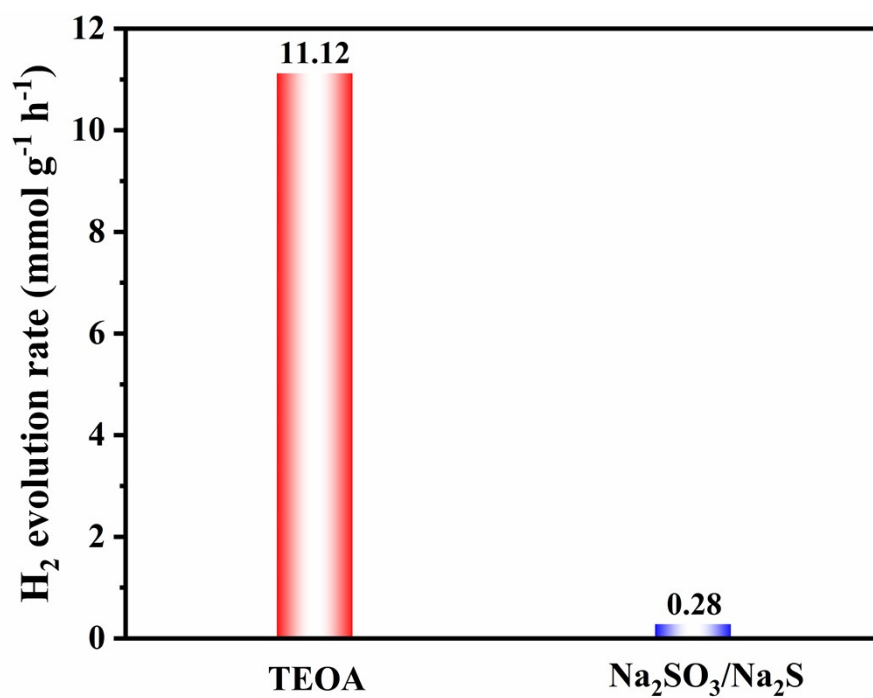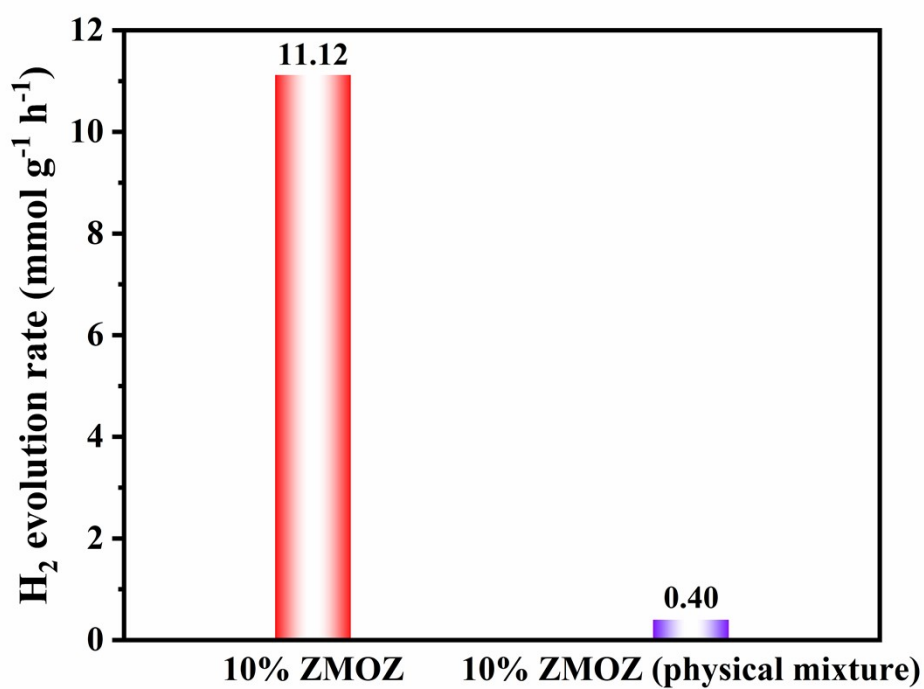| Photocatalysts	Light source	H_2 evolution rate (mmol g^{-1} h^{-1})	Cycle-index	Refs.
$Co_3O_4/ZnIn_2S_4$	300 W Xe lamp (λ>400 nm)	4.134	every 5 h reaction for 4 cycles	1
$Co_9S_8/ZnIn_2S_4$	300 W Xe lamp (λ>400 nm)	6.2	every 4 h reaction for 5 cycles	2
$Ti_3C_2T_X$ MXene@$ZnIn_2S_4$	300 W Xe lamp (λ>420 nm)	3.48	every 4 h reaction for 6 cycles	3
$ZnIn_2S_4/BiVO_4$	300 W Xe lamp (λ>400 nm)	5.9	every 5 h reaction for 4 cycles	4
$CeO_2/ZnIn_2S_4$	300 W Xe lamp (λ>400 nm)	1.5	every 3 h reaction for 4 cycles	5
Ce-doped $ZnIn_2S_4$	300 W Xe lamp (λ>420 nm)	7.4	every 4 h reaction for 4 cycles	6
$BaTiO_3@ZnIn_2S_4$	300 W Xe lamp (λ>420 nm)	8.0	/	7
$WO_3@ZnIn_2S_4$	300 W Xe lamp (λ>420 nm)	8.5	every 3 h reaction for 4 cycles	8
ZIS/CdS	300 W Xe lamp (λ>420 nm)	7.4	every 4 h reaction for 5 cycles	9
Ni-$ZnIn_2S_4$	300 W Xe lamp (λ>420 nm)	5.4	every 4 h reaction for 5 cycles	10
$NiTiO_3/ZnIn_2S_4$	300 W Xe lamp (λ>420 nm)	4.43	every 4 h reaction for 5 cycles	11
$Cu_{2-x}S@ZnIn_2S_4$	300 W Xe lamp (λ>420 nm)	4.653	every 4 h reaction for 5 cycles	12
$CuS@ZnIn_2S_4$	300 W Xe lamp (λ>400 nm)	7.91	every 4 h reaction for 5 cycles	13
$Co_2P/ZnIn_2S_4$	/	7.93	every 4 h reaction for 5 cycles	14
$MoS_2/ZnIn_2S_4$	300 W Xe lamp (λ>420 nm)	3.891	every 4 h reaction for 3 cycles	15
$ZnIn_2S_4/AgFeO_2$	300 W Xe lamp (λ>400 nm)	9.14	every 3 h reaction for 4 cycles	16
$ZnIn_2S_4/NiWO_4$	300 W Xe lamp (λ>420 nm)	1.781	every 4 h reaction for 4 cycles	17
$ZnIn_2S_4/Cu_2MoS_4$	300 W Xe lamp (λ>420 nm)	1.298	every 3 h reaction for 4 cycles	18

Photocatalysts	Light source	H$_2$ evolution rate (mmol g^{-1} h^{-1})	Cycle-index	Refs.
ZnMn$_2$O$_4$@ZnIn$_2$S$_4$	300 W Xe lamp (λ>400 nm)	11.12	every 4 h reaction for 4 cycles	This work

Table S2. The weight percentage content of Mn elements from ICP-OES.

Samples	Mn (wt%)
5% ZMOZ	0.25%
10% ZMOZ	0.42%
15% ZMOZ	1.00%
20% ZMOZ	2.50%

Table S3. BET surface area and pore volume of ZIS, ZMO and 10% ZMOZ.

Photocatalysts	BET Surface Area (m^2 g^{-1})	Pore Volume (cm^3 g^{-1})
ZIS	92.97	0.16
ZMO	44.03	0.16
10% ZMOZ	139.95	0.24

Table S4. Apparent quantum efficiencies of 10% ZMOZ at different monochromatic light irradiation.

Wavelength (nm)	H$_2$ amount (mmol)	Irradiation area (cm^2)	Light intensity (W/m^2)	Reaction time (h)	AQE (%)
380	72.22	33.18	348	2	5.47
400	75.46	33.18	430	2	4.40
420	36.86	33.18	445	2	1.98
450	20.38	33.18	450	2	1.01

Table S5. Apparent quantum efficiencies of ZIS at different monochromatic light irradiation.

Wavelength (nm)	H_2 amount (mmol)	Irradiation area (cm^2)	Light intensity (W/m^2)	Reaction time (h)	AQE (%)
380	22.17	33.18	348	2	1.69
400	29.63	33.18	430	2	1.72
420	26.64	33.18	445	2	1.43
450	9.92	33.18	450	2	0.50

References

1 G. P. Zhang, X. X. Li, M. M .Wang, X. Q. Li, Y. R. Wang, S. T. Huang, D. Y. Chen, N. J. Li, Q. F. Xu, H. Li, J. M. Lu, 2D/2D hierarchical $Co_3O_4/ZnIn_2S_4$ heterojunction with robust built-in electric field for efficient photocatalytic hydrogen evolution, *Nano Res.* 2023 **16** 6134.

2 S. B. Wang, B. Y. Guan, X. Wang, X. W. Lou, Formation of hierarchical $Co_9S_8@ZnIn_2S_4$ heterostructured cages as an efficient photocatalyst for hydrogen evolution, *J. Am. Chem. Soc.* 2018 **140** 15145.

3 G. C. Zuo, Y. T. Wang, W. L. Teo, A. M. Xie, Y. Guo, Y. X. Dai, W. Q. Zhou, D. Jana, Q. M. Xian, W. Dong, Y. L. Zhao, Ultrathin $ZnIn_2S_4$ nanosheets anchored on $Ti_3C_2T_X$ MXene for photocatalytic H_2 evolution, *Angew. Chem. Int. Ed.* 2020 **59** 11287.

4 J. D. Hu, C. Chen, Y. Zheng, G. P. Zhang, C. X. Guo, C. M. Li, Spatially Separating Redox Centers on Z-Scheme $ZnIn_2S_4/BiVO_4$ Hierarchical Heterostructure for Highly Efficient Photocatalytic Hydrogen Evolution, *Small* 2020 **16** 2002988.

5 C. L. Jiang, H. Wang, Y. Q. Wang, H. B. Ji, All solid-state Z-scheme $ZnIn_2S_4/CeO_2$ hybrid for the photocatalytic selective oxidation of aromatic alcohols coupled with hydrogen evolution, *Appl. Catal. B: Environ.* 2020 **277** 119235.

6 F. H. Tao, Y. J. Jin, K. C. Liu, W. S. Liu, One-step MOF-templated strategy to fabrication of Ce-Doped $ZnIn_2S_4$ tetrakaidecahedron hollow nanocages as an efficient photocatalyst for hydrogen evolution, *Adv. Sci.* 2022 **9** 2104579.

7 P. L. Wang, S. Y. Fan, X. Y. Li, J. Wang, Z. Y. Liu, C. P. Bai, M. O. Tadé, S. M. Liu, Piezotronic effect and hierarchical Z-scheme heterostructure stimulated photocatalytic H_2 evolution integrated with C-N coupling of benzylamine, *Nano Energy* 2021 **89** 106349.

8 S. Cao, J. G. Yu, S. Wageh, A. A. Al-Ghamdi, M. Mousavi, J. B. Ghasemi, F. Y. Xu, H_2-production and electron-transfer mechanism of a noble-metal-free $WO_3@ZnIn_2S_4$ S-scheme heterojunction photocatalyst, *J. Mater. Chem. A* 2022

10 17174.

9 C.-Q. Li, X. Du, S. Jiang, Y. Liu, Z.-L. Niu, Z.-Y. Liu, S.-S. Yi, X.-Z. Yue, Constructing Direct Z-Scheme Heterostructure by Enwrapping $ZnIn_2S_4$ on CdS Hollow Cube for Efficient Photocatalytic H_2 Generation, *Adv. Sci.* 2022 **9** 2201773.

10 B. C. Qiu, P. Huang, C. Lian, Y. X. Ma, M. Y. Xing, H. L. Liu, J. L. Zhang, Realization of all-in-one hydrogen-evolving photocatalysts via selective atomic substitution, *Appl. Catal. B Environ.* 2021 **298** 120518.

11 S. Dhingra, M. Sharma, V. Krishnan, C. M. Nagaraja, Design of noble metal-free $NiTiO_3/ZnIn_2S_4$ heterojunction photocatalyst for efficient visible-light-assisted production of H_2 and selective synthesis of 2,5-Bis(hydroxymethyl)furan, *J. Colloid Interface Sci.* 2022 **615** 346-356.

12 Y. C. Wang, M. J. Liu, C. X. Wu, J. P. Gao, M. Li, Z. P. Xing, Z. Z. Li, W. Zhou, Hollow Nanoboxes $Cu_{2-x}S@ZnIn_2S_4$ Core-Shell S-Scheme Heterojunction with Broad-Spectrum Response and Enhanced Photothermal-Photocatalytic Performance, *Small* 2022 **18** 2202544.

13 H. T. Fan, Z. Wu, K. C. Liu, W. S. Liu, Fabrication of 3D $CuS@ZnIn_2S_4$ hierarchical nanocages with 2D/2D nanosheet subunits p-n heterojunctions for improved photocatalytic hydrogen evolution, *Chem. Eng. J.* 2022 **433** 134474.

14 Q. Zhang, X. H. Wang, J. H. Zhang, L. F. Li, H. J. Gu, W.-L. Dai, Hierarchical fabrication of hollow Co_2P nanocages coated with $ZnIn_2S_4$ thin layer: Highly efficient noble-metal-free photocatalyst for hydrogen evolution, *J. Colloid Interface Sci.* 2021 **590** 632.

15 Z. Z. Zhang, L. Huang, J. J. Zhang, F. J. Wang, Y. Y. Xie, X. T. Shang, Y. Y. Gu, H. B. Zhao, X. X. Wang, In situ constructing interfacial contact $MoS_2/ZnIn_2S_4$ heterostructure for enhancing solar photocatalytic hydrogen evolution, *Appl. Catal. B Environ.* 2018 **233** 112.

16 D. Z. Kong, H. H. Fan, D. Yin, D. F. Zhang, X. P. Pu, S. J. Yao, C. H. Su, $AgFeO_2$ nanoparticle/$ZnIn_2S_4$ microsphere p-n heterojunctions with hierarchical nanostructures for efficient visible-light-driven H_2 evolution, *ACS Sustainable*

Chem. Eng. 2021 **9** 2673.

17 M. Y. Zhang, P. F. Tan, L. Yang, H. H. Zhai, H. L. Liu, J. Y. Chen, R. F. Ren, X. Y. Tan, J. Pan, Sulfur vacancy and p-n junction synergistically boosting interfacial charge transfer and separation in ZnIn$_2$S$_4$/NiWO$_4$ heterostructure for enhanced photocatalytic hydrogen evolution, *J. Colloid Interface Sci.* 2023 **634** 8170826.

18 S. K. Wang, D. F. Zhang, P. Su, X. T. Yao, J. C. Liu, X. P. Pu, H. S. Li, P. Q. Cai, In-situ preparation of mossy tile-like ZnIn$_2$S$_4$/Cu$_2$MoS$_4$ S-scheme heterojunction for efficient photocatalytic H$_2$ evolution under visible light, *J. Colloid Interface Sci.* 2023 **650** 825.